

# Generating Personalized Lower-Limb Kinematics Across Walking Speeds Using Subject-Conditioned Diffusion

Diya Dinesh\*, Adrian Krieger\*, Changseob Song, Dongho Park, Aaron J. Young, *Senior Member, IEEE*, Inseung Kang, *Member, IEEE*

**Abstract**—Personalizing exoskeleton assistance requires user-specific gait data across many locomotor tasks, yet collecting this data demands repeated motion capture sessions that are costly, time-intensive, and especially burdensome for clinical populations. This challenge is most acute across walking speeds, where gait changes substantially and deviates further in clinical gait. This work introduces a subject-conditioned residual diffusion framework that generates personalized lower-limb kinematics at unseen walking speeds from a subject’s gait sequence at a single seen speed. Given sagittal-plane hip, knee, and ankle trajectories at a seen speed and a desired unseen speed, the model generates a residual that transforms the seen trajectory into the unseen one, using a transformer denoiser conditioned on the subject’s gait and the two speeds through feature-wise linear modulation. Trained only on able-bodied data, the model achieved a mean absolute error (MAE) of  $3.4^\circ$  on held-out able-bodied subjects. Without any stroke-specific fine-tuning, it achieved a  $6.0^\circ$  MAE on out-of-training-distribution stroke subjects, retaining subject identity for clinical gait. The framework reduced the MAE by over 70% relative to supervised feed-forward baselines, and a single seen speed matched the accuracy of four speeds within  $0.4^\circ$ . These results demonstrate that subject-conditioned residual diffusion can synthesize personalized gait across speeds from minimal data, reducing the collection burden for downstream exoskeleton personalization.

**Index Terms**—Subject-conditioned diffusion, exoskeleton personalization, domain generalization, stroke gait, personalized gait generation, lower-limb kinematics.

## I. INTRODUCTION

Exoskeletons are gait-assistive devices with strong potential to improve mobility for individuals with motor impairments. [1]–[3] However, their effectiveness depends heavily on adapting to each user, since human gait varies substantially across individuals, walking speeds, impairment types, and biomechanical constraints [4]–[6]. Therefore, a one-size-fits-all controller may provide suboptimal assistance, reduce comfort, or destabilize walking. This challenge is especially important for clinical populations such as stroke survivors, where gait patterns can deviate substantially from able-bodied individuals [7]–[9]. Therefore, personalization is vital

to provide safe and effective assistance while improving the user’s functional outcomes such as energy [8]–[11], fatigue [12], [13], and stability [8], [14]–[16].

A major bottleneck for current data-driven personalization is the large amount of data required. Since each user’s gait varies across locomotor contexts [4], [5], data from a small subset of tasks may be insufficient for effective personalization. In practice, collecting gait data requires repeated motion capture sessions across tasks, such as different walking speeds. While these sessions yield high-fidelity kinematic data, they are time-consuming and exhausting for clinical populations, making it infeasible to collect the large volume of user-specific data that personalization demands.

Generative models can reduce this data overhead [17]. Instead of collecting full motion capture data across diverse locomotor tasks for each new user, generative modeling could use a single task user-gait sample to generate plausible gait data for other relevant, hard-to-extrapolate tasks. Prior motion generation work has explored generative adversarial, variational, and transformer-based models for producing realistic and temporally coherent motion [18]–[21]. Recently, diffusion models have emerged as a strong approach for motion synthesis as they provide stable training, high sample quality, and more flexible conditioning [22]–[25].

Most related to this work is GaitDynamics [25], a generative foundation model for human walking and running that jointly models center-of-mass velocities, full-body joint kinematics, and ground reaction forces over short temporal windows. GaitDynamics demonstrated capabilities relevant to exoskeleton applications, including estimating ground reaction forces from kinematics, predicting knee joint loadings, and generating plausible gait patterns across different speeds. However, GaitDynamics presents two limitations for exoskeleton personalization. First, its primary focus was population-level gait modeling rather than capturing user-specific gait characteristics. Second, it was not designed to transfer a subject-specific gait pattern across locomotor contexts, which is essential for downstream wearable robot interventions.

This leads to the main gap addressed in this paper: identity-preserving task generalization rather than an average gait representation. Here, we hypothesize that, given a short sample of a subject’s lower-limb joint angles at a single walking speed, a generative model can synthesize subject-specific gait at other speeds with biomechanical plausibility to be useful for downstream exoskeleton controller person-

\*These authors contributed equally to this work. (Corresponding author: Changseob Song, changseob@cmu.edu)

D. Dinesh is with the School of Computer Science, Carnegie Mellon University, Pittsburgh, PA, 15213 USA. A. Krieger, C. Song and I. Kang are with the Department of Mechanical Engineering, Carnegie Mellon University, USA. D. Park and A. J. Young are with the Woodruff School of Mechanical Engineering and the Institute for Robotics and Intelligent Machines, Georgia Institute of Technology, Atlanta, GA 30332 USA.

This research was supported by the NIH R21 Award 1R21EB037268-01 and NIH DP2 Award 1DP2HD111709-01.

alization. We address this gap with a subject-conditioned diffusion framework for personalized gait generation. Specifically, this work presents the following contributions: 1) a transformer-based denoiser with a subject-conditioning pipeline that combines a subject’s source-speed gait with a desired target speed; 2) a residual generation formulation that synthesizes the trajectory changes needed to transfer gait across speeds; and 3) an evaluation demonstrating identity-preserving, biomechanically plausible gait synthesis from a single source-speed sample. In doing so, the framework generates valuable user-specific data from sparse task conditions, mitigating the data collection burden inherent to downstream exoskeleton personalization workflows.

## II. METHODS

### A. Problem Design

The core task is to generate personalized lower-limb joint kinematics for a given subject across multiple walking speeds. Given a source gait sequence  $x_{src} \in \mathbb{R}^{T \times F}$  from subject  $s$  walking at a source speed  $v_{src}$ , and a desired target speed  $v_{tgt}$ , the goal is to generate a gait sequence  $\hat{x}_{tgt}$  at  $v_{tgt}$ . Here, the source sequence and the generated target sequence have the temporal dimension of  $T = 600$  data points, equivalent to 30 seconds at a sampling rate of 20 Hz, while the feature dimension  $F = 6$  captures the sagittal-plane joint angles of left and right hip, knee, and ankle joints.

The model was trained to generate the residual changes between the source and target kinematics, to better model the subtle variations across different speeds while preserving the underlying gait signatures of the user-specific source data, rather than synthesizing the raw kinematic sequence from scratch. Specifically, we generated the kinematic delta

$$\hat{r}(x_{src}, x_{tgt}) = x_{tgt} - x_{src} \quad (1)$$

Then, the target gait sequence was reconstructed as

$$\hat{x}_{tgt} = x_{src} + \hat{r}(x_{src}, x_{tgt}) \quad (2)$$

In brief, the entire diffusion pipeline learned the mapping

$$f(x_{src}, v_{src}, v_{tgt}) = \hat{r}(x_{src}, x_{tgt}). \quad (3)$$

### B. Gait Dataset

This work used an able-bodied and stroke gait dataset. The able-bodied dataset includes treadmill walking data of 22 subjects (13 males and 9 females, age  $21.6 \pm 3.6$  years, body mass  $68.5 \pm 11.33$  kg, height  $171 \pm 7$  cm) across speeds from 0.5 m/s to 1.85 m/s in 0.05 m/s increments [26]. An additional stroke dataset was collected under a protocol approved by the Georgia Institute of Technology Institutional Review Board, and all participants provided written informed consent. The dataset included 19 stroke subjects (16 males and 3 females, age  $56.6 \pm 13.7$  years, body mass  $87.46 \pm 14.69$  kg, height  $175.16 \pm 6.28$  cm, time since stroke  $97 \pm 59$  months, 11 left/8 right paretic) walking on the treadmill at 0.3, 0.6, 0.9, 1.2 m/s, and a single self-selected walking speed. All gait data was recorded at a sampling rate of 200 Hz using a marker-based motion capture system (Vicon,

Oxford, UK). Each speed trial included at least 30 seconds of level-ground walking with sagittal-plane lower-limb joint kinematics derived from motion capture.

### C. Data Preprocessing

The walking data was converted into a single 30 seconds fixed length segment for each speed trial for model training. We downsampled the 30 seconds sequences from the original 200 Hz to 20 Hz to filter out high frequency noise, resulting in 600 temporal data points.

We normalized the data using feature-wise z-score normalization. For the able-bodied data, the feature-wise mean and standard deviation were computed from the training set and subsequently applied to the train, validation, and test splits. For stroke evaluation, we computed a separate set of normalization statistics using data from 12 randomly selected stroke subjects. These stroke statistics were used only for normalization of stroke subjects and not for model training. This was done to account for distinct joint angle ranges and distributional characteristics of clinical gait, while still evaluating the model without stroke-specific fine-tuning. For both, the normalization was applied at a dataset feature-level rather than separately for each subject or speed to preserve subject identity and differences between subjects.

After preprocessing, source-target speeds were paired within each subject across walking speeds. Training pairs were generated to randomly sample across identity/same-speed pairs and cross-speed pairs, which span the entire spectrum of possible speed differences. For the held-out validation and test subjects, pairs were constructed exhaustively from all available within-subject speed combinations.

### D. Model Architecture

The generative model used in this work was a conditioned residual diffusion model, which generated the residual change needed to transform the subject’s source speed gait data into their target speed gait data (Fig. 1). The architecture had three main components outlined below.

1) *Diffusion Denoiser*: At each diffusion step  $t$ , the model took the concatenated vector of the noisy residual sample  $r_t$  and the source gait sequence  $x_{src}$  as its input. The concatenated vector had a size  $T \times 2F$ , which was 12 features per timestep. The denoiser predicted the added noise  $\hat{\epsilon}$  rather than the residual  $r_t$  directly, which follows standard diffusion model training [27]. The predicted clean residual  $\hat{r}(x_{src}, x_{tgt})$  was then added to  $x_{src}$  to generate  $\hat{x}_{tgt}$ . The diffusion denoiser was built on the transformer encoder backbone from GaitDynamics [25].

2) *Subject and Speed Conditioning*: The diffusion denoiser was conditioned on the source gait sequence of the target user, the source-target speed parameters, and the diffusion timestep. For subject conditioning, we encoded source gait data  $x_{src}$  into a lower-dimensional embedding space using a bi-directional long short-term memory encoder, and applied  $L_2$  normalization to obtain a subject embedding  $z_s$ . Here, since the subject data was conditioned directly from the source kinematic data rather than using a subject label,

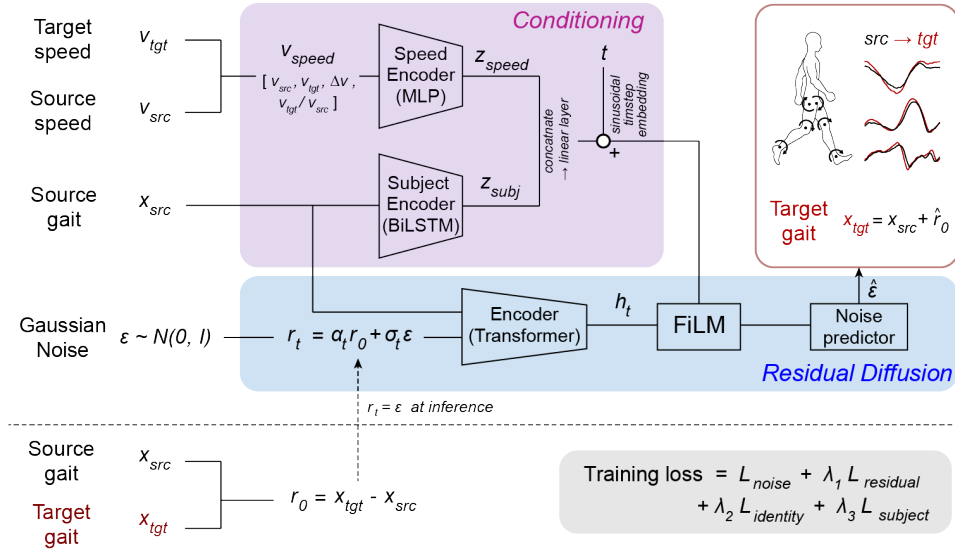


Fig. 1. **Personalized gait synthesis across walking speeds using subject-conditioned residual diffusion framework.** Given a user-specific source gait trajectory at a source speed and a desired target speed, the model generates the residual changes required to map the source gait to the target profile. The conditioning network encodes the subject’s inherent gait characteristics and velocity parameters, which are then combined with a temporal timestep embedding and integrated into the transformer denoiser via feature-wise linear modulation. The entire architecture is optimized using joint training objectives including noise prediction, residual reconstruction, identity preservation, and subject consistency.

this model can be generalized to unseen subjects at test time. To encode the relationship between the source and target velocities, we constructed the vector

$$\left[ v_{src}, v_{tgt}, v_{tgt} - v_{src}, \frac{v_{tgt}}{v_{src} + 10^{-6}} \right] \quad (4)$$

which was passed through a multilayer perceptron (MLP) to get the speed embedding  $z_{speed}$ . The subject and speed embeddings were concatenated and passed through a linear layer to form a conditioning vector  $c$ , which captures both subject-specific gait pattern and the source-to-target mapping.

At each iteration during training, a diffusion timestep  $t \in \{0, \dots, 999\}$  was sampled randomly from the 1,000 step noise schedule. This time step  $t$  was then encoded with a sinusoidal timestep embedding, where sine and cosine functions at multiple frequencies map the timestep to a higher dimension vector. This embedding was then passed through an MLP to match the conditioning dimension and was added to the subject-speed conditioning vector  $c$ . The final conditioning vector modulated the diffusion transformer encoder’s hidden states with scale and shift parameters  $(\gamma, \beta)$ , through feature-wise linear modulation (FiLM) [28]

$$\text{FiLM}(h, c) = (1 + \gamma(c)) \odot h + \beta(c) \quad (5)$$

where  $h$  is the transformer’s hidden state and  $\gamma(c)$  and  $\beta(c)$  are the scale and shift parameters produced from the conditioning vector  $c$ . FiLM allowed the subject, speed, and timestep information to shape the transformer’s hidden representation rather than directly adding these as input channels.

3) *Noise Scheduling and Training Objective:* The model was trained using a standard variance-preserving diffusion objective on the residual gait sequence  $r(x_{src}, x_{tgt})$ . At each

diffusion step  $t$ , Gaussian noise  $\epsilon \sim \mathcal{N}(0, I)$  was added to the clean residual  $r_0$  to obtain the noisy residual

$$r_t = \alpha_t r(x_{src}, x_{tgt}) + \sigma_t \epsilon \quad (6)$$

where  $\alpha_t$  and  $\sigma_t$  are determined by the variance preserving noise schedule. The denoiser was trained to predict the added noise  $\epsilon$  from  $r_t$ , while its intermediate hidden states were conditioned on the source gait, speed, and timestep through FiLM.

The training objective combined four loss terms including a weighted noise prediction loss, residual reconstruction loss, identity preservation loss, and a subject preservation loss

$$L = L_{noise} + \lambda_1 L_{residual} + \lambda_2 L_{identity} + \lambda_3 L_{subject} \quad (7)$$

where  $\lambda_i$  is a scalar weight balancing the contribution of each loss term. The primary term is a weighted mean squared error between the predicted and true diffusion noise, where knee joints were weighted twice as heavily as hip and ankle to penalize the typical higher prediction error on estimating knee joint angle [29], [30]. The residual reconstruction loss compared the reconstructed clean residual to the true residual. The identity preservation loss encouraged near-zero residuals for identity mappings ( $v_{src} = v_{tgt}$ ) and near-zero speed transitions with  $|v_{src} - v_{tgt}| < 0.1$  m/s. The subject preservation loss compared subject encoder embeddings of the source sequence  $x_{src}$  and the reconstructed generated target speed sequence  $x_{src} + \hat{r}(x_{src}, x_{tgt})$  using a batch-wise contrastive loss, where the embeddings from the same subject form positive pairs and embeddings from different subjects form negative pairs. This subject preservation loss encouraged the generated target sequences to preserve the subject-specific identity of the source data rather than collapsing into a population-average gait. The loss weights were adjusted

based on the source and target speed differences, where small differences prioritized the identity and subject consistency terms and larger cases emphasized residual reconstruction.

### E. Training and Inference

The able-bodied subjects were split into 13 training subjects, 4 validation subjects, and 5 test subjects, with no subject shared across splits. During training, we monitored the diffusion validation loss on held-out validation subjects and saved the model whenever the validation loss improved. The checkpoint with the lowest loss was used for all reported test evaluation. No explicit early stopping rule was used. Instead, the validation set was used for the checkpoint selection to prioritize the goal of generalization on unseen subjects. The training used up to 100,000 balanced source-target pairs, and validation was performed using only within-subject pairs from the validation subjects.

The model was trained using the AdamW optimizer with a learning rate of  $5 \times 10^{-4}$ , weight decay of  $10^{-3}$ , and batch size of 16. Mixed precision training and gradient clipping with a maximum norm of 1.0 were used for stability. We utilized a variance-preserving diffusion process with a 1,000-step noise schedule. Main hyperparameters included a conditioning dimension of 64 and a timestep embedding dimension of 128, built upon a 4-layer transformer denoiser backbone. At inference time, the model sampled from residual space using denoising diffusion implicit models (DDIM) sampling [31] starting from Gaussian noise. Conditioned on  $x_{src}$ ,  $v_{src}$ , and  $v_{tgt}$ , the model denoised the sample to predict  $\hat{r}(x_{src}, x_{tgt})$  over 100 steps and reconstructed the target sequence as  $\hat{x}_{tgt} = x_{src} + \hat{r}(x_{src}, x_{tgt})$ .

### F. Evaluation Metrics

Generated gait sequences were evaluated using gait cycle-normalized mean absolute error (MAE), subject personalization rank, and cadence.

1) *Mean Absolute Error*: To compare generated and real gait trajectories, we computed gait cycle-normalized MAE over lower-limb joints. Gait cycles were first identified separately for the real and generated trajectories by detecting the hip extension peaks and shifted by 50% of the detected gait cycle length to match with the nominal method based on heel-strike detection. The detected cycles were then reused for the corresponding knee and ankle joints on the same side to ensure all joints were evaluated over consistent gait-cycle boundaries. After detection, each real gait cycle was matched to a generated gait cycle greedily by selecting unused generated cycles with the closest cycle center and most similar cycle length to the real cycle. These cycles were then time-normalized to 101 points for a gait cycle percentage scale. For each joint, we averaged the normalized gait cycles for generated and real trajectories respectively, and computed the MAE between the resulting mean gait cycle trajectories for real and generated gait. The overall MAE for a single generated trajectory was then obtained by averaging the MAE values across all the lower-limb joint angles on both the right and left sides.

2) *Personalization Metric*: To evaluate how effectively the generated gait captures subject-specific features rather than population-wide averages, we compared each generated target speed trajectory against the true target speed-task data across all subjects in the dataset. For a generated sample  $\hat{x}_{tgt,s}$  for a subject at target speed, we calculated the MAE between the generated sample and the real data for every subject in our dataset at the same speed. These errors were then sorted to rank all subjects in ascending MAE order. The personalization rank is the MAE rank of the subject, where a rank closer to 1 indicates stronger subject identity preservation with the maximum rank bounded by the size of the subject cohort.

3) *Cadence*: We used cadence as a metric to evaluate how well the rhythm of the generated motion matches the target gait. It was computed as  $60 \cdot 2N/T_w$  where  $N$  is the number of gait cycles within the  $T_w$  window duration in seconds. Cadence was computed separately from the left and right hip trajectories and then averaged to obtain a single cadence value for the real and generated sequences.

### G. Baseline Models

We compared the proposed diffusion model against feed-forward MLP and temporal convolutional network (TCN) baselines trained on the same able-bodied dataset and data splits. Each training sample paired two sequences from the same subject: a reference sequence at a fixed source speed and a target sequence at another walking speed. The MLP baseline learned separate one-to-one mappings for each source-target speed pair, while the TCN baseline learned one-to-many mappings from a fixed source speed conditioned on a target speed. Both baselines used source speeds of 0.55, 0.80, 1.05, 1.30, 1.55, 1.80 m/s and were trained with AdamW and mean squared error loss on the kinematic sequences.

## III. RESULTS

### A. Overall Results

The model achieved a  $3.4^\circ$  MAE and Pearson’s correlation coefficient ( $r$ ) of 0.95 on the held-out able-bodied subjects and a  $6.0^\circ$  MAE and  $r$  of 0.86 on the stroke subjects (Table I). The average personalization rank was 3.3 out of 22 available able-bodied subjects and 2.8 out of 19 stroke subjects. Additionally, overall MAE was  $5.5^\circ$  and  $6.5^\circ$  and  $r$  was 0.86 and 0.87 for paretic and non-paretic sides, respectively (Table II). The knee joint yielded the highest error among all joints. On the paretic side, its MAE was  $2.5^\circ$  and  $1.0^\circ$  larger than the hip and ankle, respectively.

TABLE I  
OVERALL RESULTS ON ABLE-BODIED AND STROKE SUBJECTS

|                      | Able-Bodied | Stroke      |
|----------------------|-------------|-------------|
| MAE                  | $3.4^\circ$ | $6.0^\circ$ |
| $r$                  | 0.95        | 0.86        |
| Personalization rank | 3.3         | 2.8         |

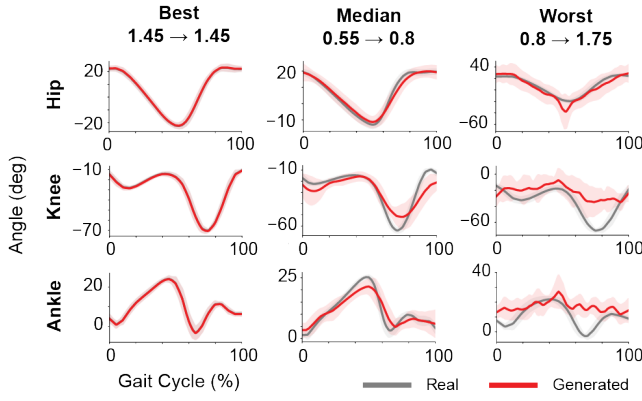


Fig. 2. **Representative able-bodied gait generation.** Comparison of ground-truth and generated joint angle trajectories over a normalized gait cycle (mean $\pm$ SD). Trajectories are presented for the best, median, and worst-performing speed pairings (source  $\rightarrow$  target speed) of the representative able-bodied subject exhibiting median overall error.

TABLE II  
KINEMATIC ACCURACY ACROSS LOWER-LIMB JOINTS

|         | MAE          |              | $r$     |             |
|---------|--------------|--------------|---------|-------------|
|         | Paretic      | Non-Paretic  | Paretic | Non-Paretic |
| Hip     | 4.1 $^\circ$ | 5.3 $^\circ$ | 0.95    | 0.93        |
| Knee    | 6.7 $^\circ$ | 8.0 $^\circ$ | 0.87    | 0.87        |
| Ankle   | 5.6 $^\circ$ | 6.3 $^\circ$ | 0.75    | 0.80        |
| Overall | 5.5 $^\circ$ | 6.5 $^\circ$ | 0.86    | 0.87        |

Similarly, on the non-paretic side, the knee MAE was 2.7 $^\circ$  and 1.7 $^\circ$  larger than the hip and ankle, respectively.

Among different generation scenarios, the best case achieved a 0.31 $^\circ$  MAE with an  $r$  of 1.00 within the (1.45, 1.45) source-target pairing (Fig. 2). The median case yielded a 3.34 $^\circ$  MAE with an  $r$  of 0.93 at the (0.55, 0.8) pairing, while the worst case had a 9.82 $^\circ$  MAE with an  $r$  of 0.65 at the (0.8, 1.75) pairing. For stroke, the best case achieved a 2.28 $^\circ$  MAE with an  $r$  of 0.99 at the (0.85, 0.85) pairing, the median case achieved a 6.15 $^\circ$  MAE with an  $r$  of 0.87 at the (0.9, 0.6) pairing, and the worst case achieved a 7.46 $^\circ$  MAE with an  $r$  of 0.84 at the (0.3, 1.2) pairing (Fig. 3). As a temporal metric for assessing adaptation to varied target speeds, the generated able-bodied cadence matched the real cadence with a 6.2 steps/min MAE, corresponding to an average percentage error of 6.8% (Fig. 4). For stroke subjects, the MAE was 5.8 steps/min, corresponding to an average percentage error of 7.4%.

### B. Personalization Rank

The average personalization rank for each source-target speed pairing across subjects is shown in the heatmap (Fig. 5). The maximum rank was 17 for one of the able-bodied subjects with source-target pairing of (1.5, 1.2) and 15 for one of the stroke subjects with the pairing of (0.3, 0.3).

### C. Speed Analysis

To determine the optimal single source speed, we compared the model's performance across different speed pairings. For both datasets, the errors were low across many

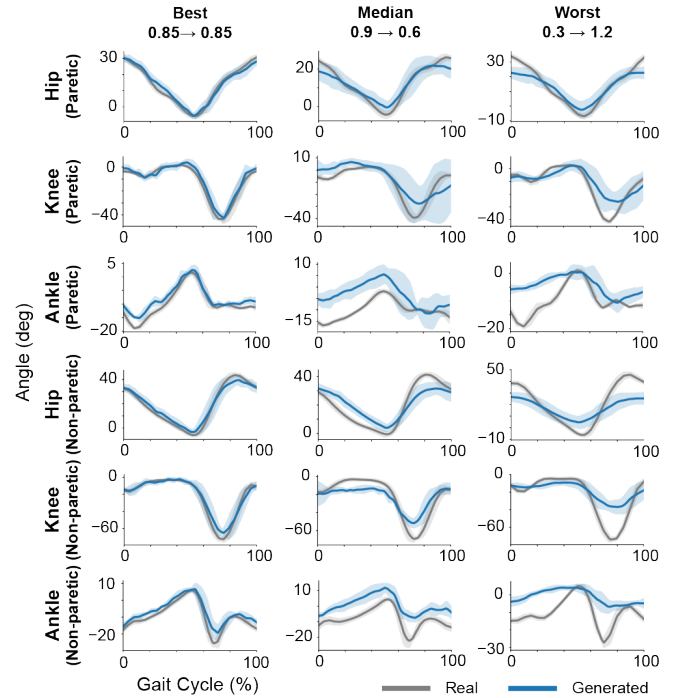


Fig. 3. **Representative stroke gait generation.** Comparison of ground-truth and generated joint angle trajectories over a normalized gait cycle for both the paretic and non-paretic limbs (mean $\pm$ SD). Trajectories are presented for the best, median, and worst performing speed pairings (source  $\rightarrow$  target speed) of the representative stroke subject exhibiting median overall error.

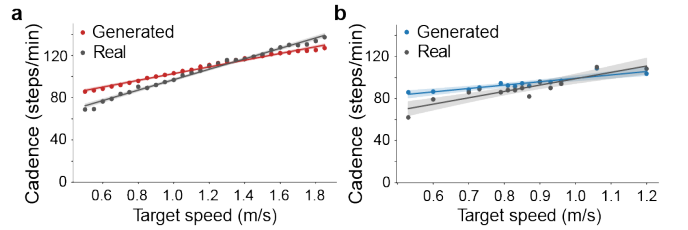


Fig. 4. **Cadence of generated gait.** Each point shows mean cadence at a target speed, aggregated across source speeds and subjects. Generated and ground-truth cadence are shown alongside regression lines and 95% confidence intervals for (a) able-bodied controls and (b) stroke individuals.

non-diagonal (non-identity) speed pairings (Fig. 6). The error remained below 5 $^\circ$  for non-diagonal pairings, with a variability of less than 1.5 $^\circ$ , while increasing alongside the source-target distance (Fig. 7c). Across all speed pairings of all able-bodied subjects, the maximum error was 22.88 $^\circ$  on the (1.45, 1.75) source-target pairing. For stroke subjects, the maximum error was 26.88 $^\circ$  on the (0.9, 0.3) pairing, a 4 $^\circ$  increase over the able-bodied worst case.

Additionally, we evaluated how source speed affects generation fidelity across all walking speeds. For able-bodied individuals, the discrepancy between the maximum and minimum MAE across all source speeds was 0.41 $^\circ$  (Fig. 7a). We also analyzed how the number of source speeds affects accuracy across all target speeds. The average MAE was 3.4 $^\circ$  with a single source speed and 3.06 $^\circ$  with four source speeds, a difference of 0.38 $^\circ$  (Fig. 7b). To assess performance when

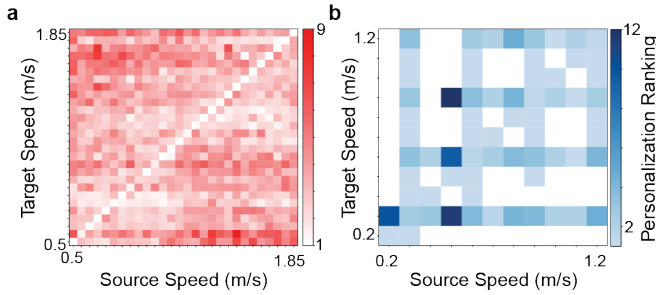


Fig. 5. **Personalization rank heatmap.** Lower ranks indicate stronger subject identity preservation, meaning the generated profile tracks closer to the true subject. Panels show results for (a) able-bodied and (b) stroke cohorts. Stroke velocities are binned to accommodate self-selected speeds, with unrepresented speed pairings shown as white cells.

TABLE III

PERSONALIZATION RANK FOR SUBJECT AND RANDOMIZED ENCODING

|             | Subject Encoding | Randomized Encoding |
|-------------|------------------|---------------------|
| Able-Bodied | 3.3              | 14.3                |
| Stroke      | 2.8              | 7.7                 |

multiple source speeds are available, we considered every possible subset of source speeds of size  $x$ . For each subset, each target speed was mapped to the closest source speed, with equidistant pairs assigned to the lower source speed. For each subset size, the final metric was computed by averaging the MAE across all target speeds per subset, followed by an average across all valid subsets of that size.

To assess how effectively the model captures subject-specific gait patterns, the personalization rank was computed by comparing subject-conditioned cases against a randomized subject-conditioned one. For the subject-conditioned case, the pipeline encoded the source gait data along with the source and target speeds. For the randomized case, a different subject was chosen randomly, and its gait trajectory was encoded together with the speed parameters. For stroke subjects, only the base speeds were used to ensure consistency. Randomizing the conditioning subject increased the personalization rank from 3.3 to 14.3 for able-bodied and from 2.8 to 7.7 for stroke subjects (Table III).

#### D. Baseline Models

The MLP and TCN baselines had average MAEs of  $12.25^\circ$  and  $11.43^\circ$ , respectively (Fig. 7a). In comparison, the proposed diffusion model achieved an average able-bodied MAE of  $3.4^\circ$ , a relative reduction of 72.2% and 70.3% over the MLP and TCN baselines.

## IV. DISCUSSION

### A. Key Findings

The main finding of this work is that subject-conditioned residual diffusion can generate target speed gait kinematics from a single source speed sequence while preserving the subject-specific gait pattern. This finding supports our hypothesis that a short sample at a single walking speed is sufficient to synthesize subject-specific gait at other speeds,

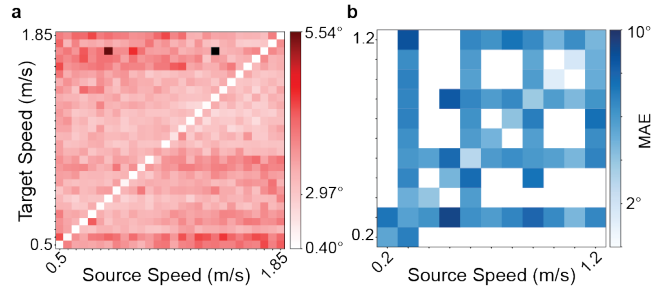


Fig. 6. **Error heatmap.** Distribution of MAE across speed pairings. (a) Error heatmap for able-bodied subjects, plotted with outliers omitted to improve readability. (b) Error heatmap for stroke subjects. Stroke velocities are binned to accommodate self-selected speeds, with unrepresented speed pairings shown as white cells.

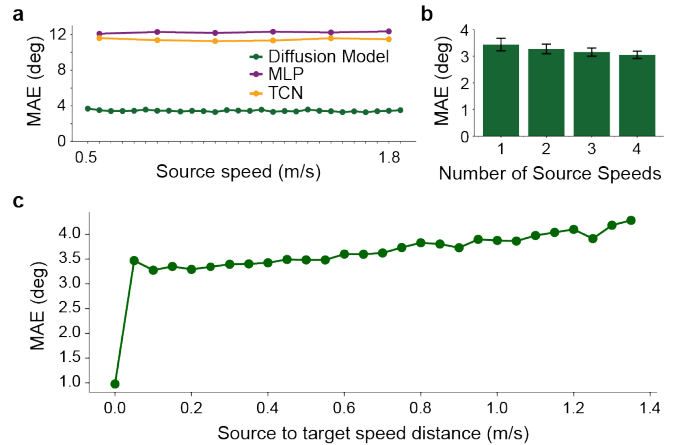


Fig. 7. **Performance under various source speed conditions.** (a) MAE per source speed for able-bodied subjects across evaluated models. (b) Impact of source speed availability on able-bodied data. For each subset size  $x$ , target speeds are mapped to the closest available source speed (defaulting to the lower speed if equidistant). Bars show the resulting average and standard deviation across all possible subsets. (c) Average able-bodied MAE as a function of the distance between source and target velocities.

suggesting that the model captures the speed-dependent gait changes without requiring data from all source speeds. On held-out able-bodied subjects, the model achieved a  $3.4^\circ$  MAE with an  $r$  of 0.95. Among lower-limb joints, the knee joints showed a higher error than the hip and ankle joints, which was also observed in other studies [29], [30]. Furthermore, the personalization ranks were low for both cohorts (3.3 and 2.8 out of 22 and 19, respectively), showing that the model preserved subject identity and effectively synthesized personalized gait.

Beyond MAE, the generated cadence trend closely followed the real trend for able-bodied subjects across target speeds, as shown by the 6.2 steps/min MAE and 6.8% average percentage error. The model was trained on able-bodied data spanning speeds from 0.5 to 1.85 m/s, while the held-out stroke data contained lower walking speeds from 0.3 to 1.2 m/s. To make the comparison more meaningful, we focused the stroke cadence analysis on speeds from 0.5 to 1.2 m/s. With this speed range, the stroke generated cadence had a 5.8 steps/min MAE and 7.4% average percentage error.

Although the stroke cadence errors were slightly larger, the generated cadence still followed the increasing target speed trend, indicating that the model captures the temporal scaling of gait in both the training-distribution able-bodied subjects and the held-out stroke subjects.

### B. Generalization to Stroke Gait

The model adapted well to stroke data, which was not included during training, across MAE, personalization, and cadence. The MAE and personalization heatmaps show that the generated trajectories preserved the subject-specific gait pattern. The generated stroke cadence closely tracked the real data, consistent with the able-bodied trends. Interestingly, MAE was lower on the paretic side than the non-paretic side overall and across specific joints. This may reflect an amplitude effect, since paretic limbs often have smaller ranges of motion, reducing the MAE. Representative gait examples show similar error levels between able-bodied and stroke data, further supporting the model’s generalization to patient data (Figs. 2 and 3).

### C. Speed Analysis and Deployment

Errors were slightly higher at extreme source-target speed pairings compared to near-identity pairings; however, increased distance from the identity line did not necessarily increase gait generation error (Fig. 6). The average error remained relatively uniform across source speeds, with a range of only  $0.41^\circ$  (Fig. 7a). Consequently, no single source speed clearly outperforms the others, confirming that the model maintains robust performance regardless of the source speed at which the user-specific sequence was collected.

To further show that a single source speed is sufficient for deployment, the average error decreased by only 4.8% from one to two source speeds, and this trend continued with additional source speeds, with only a  $0.38^\circ$  decrease between one and four (Fig. 7b). This demonstrates that one source speed is enough to generate personalized data across walking speeds and substantially decreases the data collection burden.

### D. Personalization Rank

The personalization rank showed a trend similar to the MAE, where higher ranks occurred at extreme source-target speed differences (Fig. 5). The low rank values extended beyond the diagonal, indicating that the model preserved subject-specific gait features even across non-zero speed gaps. However, as seen in the maximum error cases, the worst rank cases were not limited to the most extreme pairings, suggesting that personalization depends on subject-specific gait variation and inter-subject similarity at specific target speeds. The randomized-encoding personalization rank was substantially higher than the subject encoding rank for both able-bodied and stroke subjects (Table III). This confirms that the model does not simply generate an average target speed trajectory but uses the source gait data to personalize to each subject.

### E. Baseline Comparison

GaitDynamics is a population-level foundation model that jointly captures kinematics and kinetics across a broad range of locomotion. Our model addresses a complementary objective: conditioning on user-specific source data to preserve subject identity and extrapolating to patient populations, both of which fall outside GaitDynamics’ population-level scope [25]. For the MLP and TCN baselines, personalized gait synthesis across speeds was not well captured by simple, deterministic mappings. The substantially higher baseline MAEs compared to our proposed model show that residual diffusion better captures nonlinear, subject-specific gait changes across walking speeds.

### F. Limitations

One limitation we faced was a limited number of stroke subjects and their speed pairings available for training, testing, and potential downstream model fine-tuning. Similarly, the personalization rank metric was dependent on the availability of comparable subjects at the target speed. We also acknowledge that the kinematic MAE did not directly reflect the performance of exoskeleton control. We have not directly tested how our pipeline works in downstream tasks, examples of which are imitation-learned user-specific digital twins in physics-informed simulations to train exoskeleton control policies [32]–[34] and kinematics-based lower-limb prosthetic controllers during swing phase [35], [36].

### G. Future Work

Future work will scale to a larger number of stroke subjects with larger inter-subject variability. We will also synthesize a wider range of daily locomotor tasks such as ramp or stair walking. Furthermore, since this study was limited to sagittal-plane motion analysis, we will work on generating motions in the frontal and transverse planes, considering that stroke patients largely suffer from hip circumduction. We are also interested in expanding this pipeline into estimating unmeasured user-specific kinetic or muscle activation profiles, since these modalities inform the user’s internal physiological state and can be directly utilized for downstream exoskeleton applications and biomechanical monitoring. Additionally, computer vision-based pose and kinematics estimation pipelines have recently seen significant improvements [37]–[39]. Future work can leverage these pipelines to collect source kinematics without using any professional motion capture equipment.

## V. CONCLUSION

This work introduced a subject-conditioned residual diffusion framework for personalized gait generation. By conditioning a transformer denoiser on subject gait data at a source speed and a desired target speed, the model generated lower-limb kinematics while preserving subject identity. The model achieved a  $3.4^\circ$  MAE on unseen able-bodied subjects, generalized to out-of-distribution stroke subjects without fine-tuning, and outperformed deterministic MLP and TCN

baselines. These results demonstrate that the residual diffusion framework can reduce the motion capture data required for exoskeleton personalization by enabling target speed gait data generation from limited source data.

## REFERENCES

- [1] G. S. Sawicki, O. N. Beck, I. Kang, and A. J. Young, "The exoskeleton expansion: improving walking and running economy," *Journal of neuroengineering and rehabilitation*, vol. 17, no. 1, p. 25, 2020.
- [2] C. Sivy *et al.*, "Opportunities and challenges in the development of exoskeletons for locomotor assistance," *Nature biomedical engineering*, vol. 7, no. 4, pp. 456–472, 2023.
- [3] S. Gao *et al.*, "Wearable technologies for assisted mobility in the real world," *Nature Communications*, vol. 16, Dec. 2025.
- [4] D. A. Winter, "Kinematic and kinetic patterns in human gait: Variability and compensating effects," *Human Movement Science*, vol. 3, p. 51–76, Mar. 1984.
- [5] K. Son, J. Park, and S. Park, "Variability analysis of lower extremity joint kinematics during walking in healthy young adults," *Medical Engineering & Physics*, vol. 31, p. 784–792, Mar. 2009.
- [6] K. R. Embry, D. J. Villarreal, R. L. Macaluso, and R. D. Gregg, "Modeling the kinematics of human locomotion over continuously varying speeds and inclines," *IEEE Transactions on Neural Systems and Rehabilitation Engineering*, vol. 26, p. 2342–2350, Dec. 2018.
- [7] B. Balaban and F. Tok, "Gait disturbances in patients with stroke," *PM&R*, vol. 6, p. 635–642, Jan. 2014.
- [8] L. N. Awad *et al.*, "A soft robotic exosuit improves walking in patients after stroke," *Science Translational Medicine*, vol. 9, July 2017.
- [9] I. Kang *et al.*, "Online adaptation framework enables personalization of exoskeleton assistance during locomotion in patients affected by stroke," *IEEE Transactions on Robotics*, vol. 41, p. 4941–4959, 2025.
- [10] K. Pruyne, R. Murray, L. Gabert, K. B. Foreman, and T. Lenzi, "Portable hip exoskeleton improves walking economy for stroke survivors," *Nature Communications*, vol. 17, Feb. 2026.
- [11] A. J. Gunnell *et al.*, "Powered knee exoskeleton improves sit-to-stand transitions in stroke patients using electromyographic control," *Communications Engineering*, vol. 4, June 2025.
- [12] N. V. Divekar, E. H. Hinojosa, J. Zhang, and R. D. Gregg, "A task-agnostic knee exoskeleton for reducing osteoarthritis pain across activities of daily life: A pilot study," in *2025 International Conference On Rehabilitation Robotics (ICORR)*, p. 1437–1443, May 2025.
- [13] J. Zhang, N. V. Divekar, E. H. Hinojosa, and R. D. Gregg, "A task-agnostic hip exoskeleton for osteoarthritis pain relief: Energetic control across activities of daily life," in *2025 International Conference On Rehabilitation Robotics (ICORR)*, p. 1299–1306, May 2025.
- [14] D. Archangeli *et al.*, "Exoskeleton frontal and sagittal plane hip torque improves propulsion and transient stability during walking in individuals with hemiparesis," *Journal of NeuroEngineering and Rehabilitation*, May 2026.
- [15] Z. F. Lerner, D. L. Damiano, and T. C. Bulea, "A lower-extremity exoskeleton improves knee extension in children with crouch gait from cerebral palsy," *Science Translational Medicine*, vol. 9, no. 404, p. eaam9145, 2017.
- [16] J. Kim *et al.*, "Soft robotic apparel to avert freezing of gait in parkinson's disease," *Nature Medicine*, vol. 30, p. 177–185, Jan. 2024.
- [17] L. Manduchi *et al.*, "On the challenges and opportunities in generative AI," Feb. 2024.
- [18] E. Barsoum, J. Kender, and Z. Liu, "Hp-gan: Probabilistic 3d human motion prediction via gan," in *2018 IEEE/CVF Conference on Computer Vision and Pattern Recognition Workshops (CVPRW)*, pp. 1499–149909, IEEE, 2018.
- [19] M. Petrovich, M. J. Black, and G. Varol, "Action-conditioned 3d human motion synthesis with transformer vae," in *2021 IEEE/CVF International Conference on Computer Vision (ICCV)*, pp. 10965–10975, 2021.
- [20] C. Guo *et al.*, "Action2motion: Conditioned generation of 3d human motions," in *Proceedings of the 28th ACM International Conference on Multimedia (MM '20)*, pp. 2027–2035, 2020.
- [21] T. Lucas, F. Baradel, P. Weinzaepfel, and G. Rogez, "Posegpt: Quantization-based 3d human motion generation and forecasting," in *European Conference on Computer Vision (ECCV)*, 2022.
- [22] M. Zhang *et al.*, "Motiondiffuse: Text-driven human motion generation with diffusion model," *IEEE Transactions on Pattern Analysis and Machine Intelligence*, vol. 46, no. 6, pp. 4115–4128, 2024.
- [23] G. Tevet, O. Gordon, R. Shalev, and A. H. Bermano, "Motionclip: Exposing human motion generation to clip space," *arXiv*, 2023.
- [24] Y. Duan, W. Luo, D. Yu, X. Peng, and J. S. Ren, "Diffmotion: Synthesizing diverse and physically plausible human motion using diffusion models," *arXiv*, 2024.
- [25] T. Tan *et al.*, "GaitDynamics: a generative foundation model for analyzing human walking and running," *Nature Biomedical Engineering*, Jan. 2026.
- [26] J. Camargo, A. Ramanathan, W. Flanagan, and A. Young, "A comprehensive, open-source dataset of lower limb biomechanics in multiple conditions of stairs, ramps, and level-ground ambulation and transitions," *Journal of Biomechanics*, vol. 119, p. 110320, Apr. 2021.
- [27] J. Ho, A. Jain, and P. Abbeel, "Denoising diffusion probabilistic models," *arXiv*, 2020.
- [28] E. Perez, F. Strub, H. de Vries, V. Dumoulin, and A. Courville, "FiLM: Visual reasoning with a general conditioning layer," *arXiv*, 2017.
- [29] S. Sivakumar, A. A. Gopalai, K. H. Lim, D. Gouwanda, and S. Chauhan, "Joint angle estimation with wavelet neural networks," *Scientific Reports*, vol. 11, p. 10306, may 2021.
- [30] J. Li, K. Zhu, D. Li, P. Kang, and P. B. Shull, "3d knee and hip angle estimation with reduced wearable imus via transfer learning during yoga, golf, swimming, badminton, and dance," *IEEE Transactions on Neural Systems and Rehabilitation Engineering*, vol. 32, p. 325–338, 2024.
- [31] J. Song, C. Meng, and S. Ermon, "Denoising diffusion implicit models," in *International Conference on Learning Representations*, 2021.
- [32] I. Choi, I. Park, E. Halilaj, and I. Kang, "Musculoskeletal motion imitation for learning personalized exoskeleton control policy in impaired gait," *arXiv*, 2026.
- [33] Y.-H. Chiu, U. H. Lee, C. Song, M. Hu, and I. Kang, "Learning speed-adaptive walking agent using imitation learning with physics-informed simulation," in *2025 International Conference On Rehabilitation Robotics (ICORR)*, pp. 835–841, IEEE, 2025.
- [34] G. Leem, J. Lee, J. Lee, S. Song, and J. Won, "Exo-plore: Exploring exoskeleton control space through human-aligned simulation," *arXiv*, 2026.
- [35] M. Tran, L. Gabert, S. Hood, and T. Lenzi, "A lightweight robotic leg prosthesis replicating the biomechanics of the knee, ankle, and toe joint," *Science Robotics*, vol. 7, Nov. 2022.
- [36] D. Quintero, D. J. Villarreal, D. J. Lambert, S. Kapp, and R. D. Gregg, "Continuous-phase control of a powered knee–ankle prosthesis: Amputee experiments across speeds and inclines," *IEEE Transactions on Robotics*, vol. 34, p. 686–701, June 2018.
- [37] S. Gilon, E. Y. Miller, and S. D. Uhlrich, "OpenCap monocular: 3d human kinematics and musculoskeletal dynamics from a single smartphone video," *arXiv*, 2026.
- [38] C. Song, B. Ivanyuk-Skulskiy, A. Krieger, K. Luo, and I. Kang, "Personalization of wearable sensor-based joint kinematics estimation using computer vision for hip exoskeleton applications," in *2025 International Conference On Rehabilitation Robotics (ICORR)*, p. 534–539, May 2025.
- [39] R. M. Kanko, E. Laende, W. S. Selbie, and K. J. Deluzio, "Inter-session repeatability of markerless motion capture gait kinematics," *Journal of Biomechanics*, vol. 121, p. 110422, 2021.